Mon. Not. R. Astron. Soc. **350,** 1485–1494 (2004) doi:10.1111/j.1365-2966.2004.07751.x

The 2dF galaxy redshift survey: clustering properties of radio galaxies

Manuela Magliocchetti,[1⋆] Steve J. Maddox,[2] Ed Hawkins,[2] John A. Peacock,[3] Joss Bland-Hawthorn,[4] Terry Bridges,[4] Russell Cannon,[4] Shaun Cole,[5] Matthew Colless,[6] Chris Collins,[7] Warrick Couch,[8] Gavin Dalton,[10] Roberto de Propris,[8] Simon P. Driver,[9] George Efstathiou,[11] Richard S. Ellis,[12] Carlos S. Frenk,[5] Karl Glazebrook,[13] Carole A. Jackson,[6] Bryn Jones,[3] Ofer Lahav,[11] Ian Lewis,[5] Stuart Lumsden,[14] Peder Norberg,[15] Bruce A. Peterson,[4] Will Sutherland[3] and Keith Taylor[4] (the 2dFGRS Team)

[1] *SISSA, Via Beirut 4, 34100, Trieste, Italy*
[2] *School of Physics and Astronomy, University of Nottingham, Nottingham NG7 2RD*
[3] *Institute for Astronomy, University of Edinburgh, Royal Observatory, Blackford Hill, Edinburgh EH9 3HJ*
[4] *Anglo-Australian Observatory, PO Box 296, Epping, NSW 2121, Australia*
[5] *Department of Physics, University of Durham, South Road, Durham DH1 3LE*
[6] *Research School of Astronomy and Astrophysics, The Australian National University, Canberra, ACT 2611, Australia*
[7] *Astrophysics Research Institute, Liverpool John Moores University, Twelve Quays House, Birkenhead, L14 1LD*
[8] *Department of Astrophysics, University of New South Wales, Sydney, NSW 2052, Australia*
[9] *School of Physics and Astronomy, University of St Andrews, North Haugh, St Andrews, Fife KY6 9SS*
[10] *Department of Physics, University of Oxford, Keble Road, Oxford OX1 3RH*
[11] *Institute of Astronomy, University of Cambridge, Madingley Road, Cambridge CB3 0HA*
[12] *Department of Astronomy, California Institute of Technology, Pasadena, CA 91125*
[13] *Department of Physics and Astronomy, Johns Hopkins University, Baltimore, MD 21218-2686, USA*
[14] *Department of Physics, University of Leeds, Woodhouse Lane, Leeds LS2 9JT*
[15] *ETHZ Institut für Astronomie, HPF G3.1, ETH Hönggerberg, CH-8093 Zürich, Switzerland*

Accepted 2004 February 18. Received 2004 February 6; in original form 2003 October 30

ABSTRACT

The clustering properties of local, $S_{1.4\,\mathrm{GHz}} \geqslant 1$ mJy, radio sources are investigated for a sample of 820 objects drawn from the joint use of the Faint Images of the Radio Sky at 20 cm (FIRST) and 2dF Galaxy Redshift surveys. To this aim, we present 271 new $b_\mathrm{J} \leqslant 19.45$ spectroscopic counterparts of FIRST radio sources to be added to those already introduced in our previous paper. The two-point correlation function for the local radio population is found to be entirely consistent with estimates obtained for the whole sample of 2dFGRS galaxies. From measurements of the redshift-space correlation function $\xi(s)$ we derive a redshift-space clustering length $s_0 = 10.7^{+0.8}_{-0.7}$ Mpc, while from the projected correlation function $\Xi(r_\mathrm{T})$ we estimate the parameters of the real-space correlation function $\xi(r) = (r/r_0)^{-\gamma}$, $r_0 = 6.7^{+0.9}_{-1.1}$ Mpc and $\gamma = 1.6 \pm 0.1$, where $h = 0.7$ is assumed. Different results are instead obtained if we only consider sources that present signatures of active galactic nucleus (AGN) activity in their spectra. These objects are shown to be very strongly correlated, with $r_0 = 10.9^{+1.0}_{-1.2}$ Mpc and $\gamma = 2 \pm 0.1$, a steeper slope than has been claimed in other recent works. No difference is found in the clustering properties of radio-AGNs of different radio luminosity. Comparisons with models for $\xi(r)$ show that AGN-fuelled sources reside in dark matter haloes more massive than $\sim 10^{13.4}$ $\mathrm{M}_\odot$, higher than the corresponding figure for radio-quiet quasi-stellar objects. This value can be converted into a minimum black hole mass associated with radio-loud, AGN-fuelled objects of $M_\mathrm{BH}^\mathrm{min} \sim 10^9$ $\mathrm{M}_\odot$. The above results then suggest – at least for relatively faint radio objects – the existence of a threshold black hole mass associated with the onset of significant radio activity such as that of radio-loud AGNs; however, once the activity is triggered, there appears to be no evidence for a connection between black hole mass and level of radio output.

Key words: galaxies: active – galaxies: distances and redshifts – galaxies: starburst – galaxies: statistics – cosmology: observations – radio continuum: galaxies.

1 INTRODUCTION

In the last 20 yr, radio sources have been shown to be extremely good probes of cosmological large-scale structure up to significant ($z \sim 4$) redshifts. Clustering in radio catalogues was detected in early wide-area studies: Seldner & Peebles (1981) and Shaver & Pierre (1989) reported on the detection of slight clustering of nearby radio sources, while Kooiman, Burns & Klypin (1995) and Loan, Wall & Lahav (1997) measured strong anisotropy in the distribution of bright radio objects from the 4.85-GHz Green Bank and Parkes/Massachusetts Institute of Technology (MIT)/National Radio Astronomy Observatories (NRAO) surveys. However, it was only a few years ago that the latest generation of radio surveys, such as Faint Images of the Radio Sky at 20 cm (FIRST; Becker, White & Helfand 1995), the Westerbork Northern Sky Survey (WENSS; Rengelink et al. 1998) and the NRAO Very Large Array (VLA) Sky Survey (NVSS; Condon et al. 1998), included enough objects to allow for high-precision clustering measurements (Cress et al. 1996; Magliocchetti et al. 1998; Rengelink et al. 1998; Blake & Wall 2003; Overzier et al. 2003). All these recent analyses reveal the tendency for radio objects to be more strongly clustered than optically-selected galaxies.

Assessing the real clustering signal is nevertheless not an easy task when it comes to radio sources, because the lack of known redshifts for the overwhelming majority of these objects forces one to deal with projected quantities such as the angular two-point correlation function $w(\theta)$. Unfortunately, the relation between angular and spatial measurements is dependent on the radio source redshift distribution $N(z)$ – which is highly uncertain at the mJy flux levels probed by these new surveys (see, for example, Dunlop & Peacock 1990; Magliocchetti et al. 1999) – and on the unknown redshift evolution of the radio clustering signal. This leads to estimates for the comoving correlation length r_0 [here we are assuming the spatial two-point correlation function to be described by the power law $\xi(r) = (r/r_0)^{-\gamma}$] which may span the relatively broad range ∼7–15 Mpc even for angular measurements in good agreement with each other (Magliocchetti et al. 1998; Blake & Wall 2003; Overzier et al. 2003).

Because the natural solution to the above problem (redshift acquisition for all the objects included in a chosen catalogue) is out of reach with current instruments, a good starting point towards the understanding of the clustering properties of radio sources is the analysis of homogeneous subsamples of objects, bright enough in the visible band to allow for optical and spectroscopic follow-ups.

A first attempt in this direction was performed by Peacock & Nicholson (1991) who measured the redshift-space correlation function for a sample of 310 radio galaxies with $z \lesssim 0.1$ and radio fluxes $S > 0.5$ Jy at 1.4 GHz. These authors indeed found radio sources in their catalogue to be strongly clustered, with a redshift-space correlation length $s_0 \simeq 11\ h^{-1}$ Mpc.

The present paper analyses the clustering properties of ∼820, $z \lesssim 0.3$, $S_{1.4\,\mathrm{GHz}} \geqslant 1$ mJy radio galaxies drawn from the joint use of the FIRST survey and the 2dF Galaxy Redshift Survey (2dFGRS), as illustrated in Magliocchetti et al. (2002). By doing this, we not only extend the Peacock & Nicholson (1991) measurements to a statistically more significant sample involving less local objects, but we also probe much lower flux densities where the population contains radio-emitting sources that differ from typical AGNs (such as galaxies undergoing intense star formation).

In addition to the above analysis, we will also estimate the two-point correlation function (both in redshift space and real space) for the homogeneous sample of radio-AGNs (sources that present signatures of AGN activity in their optical spectra). This will enable us to use up-to-date models, which connect galaxy formation properties with clustering behaviour in order to investigate the nature of the dark matter haloes in which these sources reside. By means of the same approach, we can also obtain precious information on the nature of the black hole associated with a radio-active AGN to be compared with conclusions from other works.

For instance, Auriemma et al. (1977) found that radio emission is more common in brighter/more massive ellipticals. This result was recently confirmed, for example, by findings of Falomo, Carangelo & Treves (2003), while authors such as Laor (2000), Lacy et al. (2001), McLure & Dunlop (2002), McLure & Jarvis (2002) and Dunlop et al. (2003) have investigated the connection between black hole mass and radio luminosity, coming to conclusions in disagreement with each other.

The layout of the paper is as follows. In Section 2 we introduce 271 new spectroscopic counterparts for local, $S_{1.4\,\mathrm{GHz}} \geqslant 1$ mJy, radio sources, derived from the joint use of the FIRST survey and the 2dFGRS. In Section 3.1 we describe some of the properties of the total FIRST–2dFGRS sample, which puts together objects presented in Section 2 with those introduced in Magliocchetti et al. (2002). Sections 3.2 and 3.3 are respectively devoted to the analysis of the redshift-space correlation function $\xi(s)$ and of the projected correlation function $\Xi(r_\mathrm{T})$ both for the whole radio 2dFGRS sample and only for the 536 radio-AGNs. In Section 4 we compare the available data with models in order to derive the minimum dark matter mass of a halo able to host an AGN-fuelled radio source and we give some constraints on the minimum black hole mass of a radio-loud AGN. Finally, in Section 5 we summarize our conclusions.

Unless stated otherwise, throughout this work we will assume $\Omega_0 = 0.3$, $\Lambda = 0.7$, $h = 0.7$ and $\sigma_8 = 0.8$ (where σ_8 is the rms density fluctuation within a sphere with a radius of 8 h^{-1} Mpc), as the latest results from the joint analysis of cosmic microwave background (CMB) and 2dFGRS data seem to indicate (see, for example, Lahav et al. 2002; Spergel et al. 2003). To avoid confusion, we especially emphasize that distances will thus normally be quoted in Mpc, assuming $h = 0.7$. Units of h^{-1} Mpc will occur only rarely. This assumption is also made in all figures quoted for radio luminosities and black hole masses. All the correlation lengths are in comoving units.

2 MORE SPECTROSCOPIC COUNTERPARTS FOR FIRST RADIO SOURCES

The 2dFGRS (Colless et al. 2001, 2003) is a large-scale survey selected in the photometric b_J band from the Automated Plate Measuring (APM) catalogue (Maddox et al. 1990a,b; Maddox, Efstathiou & Sutherland 1996) and its subsequent extensions (Maddox et al., in preparation). The final version includes 221 414 unique, reliable (i.e. with quality flags $Q \geqslant 3$; Colless et al. 2001, 2003) galaxy redshifts to an extinction-corrected limit for completeness of $b_\mathrm{J} \simeq 19.45$ (with small variations in magnitude limit as a function of position over the sky) over an area of 2151 deg^2. The survey geometry consists of two broad declination strips, a larger one in the South Galactic Pole (SGP) covering the area $3^\mathrm{h}30^\mathrm{m} \lesssim \mathrm{RA(2000)} \lesssim 21^\mathrm{h}40^\mathrm{m}$, $-37^\circ.5 \lesssim \mathrm{Dec.(2000)} \lesssim -22^\circ.5$ and a smaller one set in the North Galactic Pole (NGP) with $9^\mathrm{h}50^\mathrm{m} \lesssim \mathrm{RA(2000)} \lesssim 14^\mathrm{h}50^\mathrm{m}$, $2^\circ.5 \lesssim \mathrm{Dec.(2000)} \lesssim -7^\circ.5$, plus 100 random two-degree fields (2dFs) spread uniformly over the 7000 deg^2 of the APM catalogue in the southern Galactic hemisphere. The median redshift of the galaxies is 0.11 and the great majority have $z < 0.3$.

The completion of the 2dFGRS has allowed us to obtain 271 new spectroscopic counterparts for $S_{1.4\,\mathrm{GHz}} \geqslant 1$ mJy radio objects to be added to the sample presented in Magliocchetti et al. (2002). As in Magliocchetti et al. (2002), the parent radio data set comes from matching together sources in the FIRST (Becker et al. 1995) and APM catalogues over the region of the sky between $9^{\mathrm{h}}48^{\mathrm{m}} \lesssim \mathrm{RA(2000)} \lesssim 14^{\mathrm{h}}32^{\mathrm{m}}$ and $-2.^{\circ}77 \lesssim \mathrm{Dec.(2000)} \lesssim 2.^{\circ}25$, where these two surveys overlap. Magliocchetti & Maddox (2002) find 4075 identifications – corresponding to 16.7 per cent of the original radio sample – in the APM catalogue for $b_{\mathrm{J}} \leqslant 22$ and for a matching radius of 2 arcsec, a value chosen as the best compromise to maximize the number of real associations (expected to be ∼9 per cent of the FIRST–APM data set), while limiting the number of random coincidences to a negligible ∼5 per cent. 971 objects (hereafter indicated as the photometric catalogue) in the parent data set exhibit b_{J} magnitudes brighter than 19.45, the limit of the 2dFGRS.

We note that, even though the fine angular resolution of the FIRST survey implies that some of the flux coming from extended sources could be either resolved out or split into two or more components, leading to a systematic underestimate of the real flux densities of such sources, this effect has been partially corrected for by using the method developed by Magliocchetti et al. (1998) to combine multicomponent objects. The above technique, together with the matching procedure, associates optical counterparts to the centroids of multicomponent sources, thus minimizing the chances of missing an object with extended radio emission. Also, as already discussed in Magliocchetti et al. (2002), the correction to radio fluxes as measured by FIRST is ∼1 mJy in the case of sources brighter than 3 mJy, and about 30 per cent for sources with $1 \leqslant S_{1.4\,\mathrm{GHz}} \lesssim 3$ mJy (which mainly correspond to compact spiral galaxies and starbursts). These corrections have been shown not to affect any of the results obtained in both the previous (Magliocchetti et al. 2002) and current works.

The new spectroscopic counterparts were identified by searching in the 2dFGRS catalogue for objects not yet present in the Magliocchetti et al. (2002) sample with positions that differed by less than 2 arcsec (the value of the diameter of each 2dF fibre) from positions of sources in the parent photometric data set. The properties of these 271 objects are described in the complete, online version of Table 1 (a sample is shown here). For each of them the table indicates:

(1) source number;
(2) right ascension α (J2000);
(3) declination δ (J2000) as measured in the 2dFGRS;
(4) offset (expressed in arcsec) between radio and optical counterpart in the APM catalogue;
(5) radio-flux density (in mJy units) at 1.4 GHz;
(6) apparent b_{J};
(7) when present, R magnitudes of the optical counterpart;
(8) redshift;
(9) spectral classification.

Following Magliocchetti et al. (2002), classes for the optical counterparts of radio sources (column 9 of Table 1) have been assigned on the basis of their 2dF spectra. Spectra have been compared with known templates (see, for example, Kennicut, 1992; McQuade, Calzetti & Kinney 1995) which allowed galaxies to be divided into six broad categories, as follows.

(1) *Early-type galaxies*. 150 sources where spectra were dominated by continua much stronger than the intensity of any emission line. These objects can be further divided into two subclasses:

(i) galaxies with absorption lines only;

(ii) galaxies with absorption lines + weak [O SC ii] and Hα emission lines denoting little star formation activity.

(2) *E+AGN-type galaxies*. 40 sources showing spectra typical of early-types plus the presence of (narrow) emission lines such as [O II], [O III], [N II] and [S II], which are strong if compared to any Balmer line in emission and indicate the presence of large, partially ionized transition regions, as is the case in active galaxies.

(3) *Late-type galaxies*. 51 sources where spectra show strong emission (mainly Balmer) lines characteristic of star formation activity, together with a detectable continuum.

(4) *Starburst galaxies*. 15 sources with optical spectra characterized by an almost negligible continuum with very strong emission lines indicating the presence of intense star formation activity.

(5) *Seyfert 1 galaxies*. One source with spectrum showing strong, broad emission lines.

(6) *Seyfert 2 galaxies*. Nine sources where the continuum is missing and spectra only show strong narrow emission lines due to the presence of an AGN.

Distinctions between different classes of sources and in particular between E+AGN, Seyfert 2 and late-type galaxies have relied on the diagnostic emission-line ratios of Veilleux & Osterbrock (1987), Woltjer (1990) and Rola, Terlevich & Terlevich (1997). Note that a definite classification was not possible for all the cases. This simply reflects the fact that it is, in general, quite common to find 'composite' galaxies containing both an AGN and ongoing star formation (see, for example, Hill et al. 2001). We also found two intermediate cases of Seyfert 2 spectral types with mildly broadened emission lines.

More details on the properties of the full FIRST–2dFGRS sample are given in Section 3.1.

3 CLUSTERING PROPERTIES OF LOCAL RADIO SOURCES

3.1 Data set

The combination of the sample introduced in Magliocchetti et al. (2002) and of those sources presented in Section 2 provides us with a total of 828 FIRST radio objects with a spectroscopic counterpart in the 2dFGRS. This number is reduced to 820 if we only consider spectra with quality flag $Q \geqslant 3$ and discard the (four) stars present in the data set. Their projected distribution on to the sky is shown in Fig. 1, whereby empty circles identify the 971 $b_{\mathrm{J}} \leqslant 19.45$ and $S \geqslant 1$ mJy sources drawn from the parent photometric catalogue (see Section 2), while filled dots represent the 820 objects with available redshift estimates and spectral classifications.

In order to investigate the radio properties of the sample, Figs 2 and 3 respectively show b_{J} magnitudes versus radio flux S at 1.4 GHz and radio power distribution. In more detail, the left-hand panel of Fig. 2 is devoted to the b_{J}–S distribution of 'classical', AGN-powered sources (hereafter called radio-AGNs), while the right-hand panel was obtained for the subclass of star-forming galaxies which owe their radio emission to processes different from accretion on to a central black hole. Empty circles then are for early-type galaxies, filled dots for E+AGN-type galaxies, crosses for Seyfert galaxies (regardless of whether type 1 or 2), while filled triangles are for late-type galaxies and filled squares for starbursts, where the classification follows that introduced in Section 2. The dashed lines in both panels indicate the loci of constant radio-to-optical ratios $r = S \times 10^{(b_{\mathrm{J}}-12.5)/2.5}$, and the dotted lines illustrate the threshold of $r \sim 30$ for an object to be considered as radio-loud. It is clear

Table 1. Sample table of the full list of spectral identifications, which is available in the online version of the article at http://www.blackwellpublishing.com/products/journals/suppmat/MNR/MNR7751/mnr7751sm.htm.

Object	α (J2000)	δ (J2000)	Off	S1.4	*bJ*	R	z	Class
270395	10 31 56.79	+1 30 44.6	0.81	7.98	18.15	15.86	0.1868	Early
270654	10 30 40.00	+1 1 13.4	1.03	1.27	17.85	16.28	0.1313	Late
271177	10 27 56.11	+1 51 32.9	1.46	8.13	18.89	17.53	0.1508	Early
271274	10 27 25.03	+1 14 29.9	0.47	3.04	16.16	15.26	0.0224	E+AGN
271688	10 25 52.06	+1 11 27.3	1.77	16.79	16.17	14.66	0.0961	Early
271709	10 25 45.13	+1 34 10.5	0.83	3.03	18.54	16.42	0.1861	Early
271833	10 25 15.25	+1 38 30.5	0.11	6.68	17.72	15.91	0.0927	Early
272373	10 22 50.49	-1 27 18.1	0.95	4.28	16.84	15.80	0.0962	Early
272518	10 22 17.81	-1 56 0.3	0.32	2.92	18.60	17.54	0.1128	Late
272848	10 21 8.19	-0 51 20.0	0.69	1.13	17.76	16.52	0.1269	E+AGN
272943	10 20 48.51	+2 6 42.1	0.50	1.88	16.56	14.49	0.0729	Early
273133	10 20 8.08	-0 47 51.5	0.53	5.58	16.79	15.85	0.0564	Late

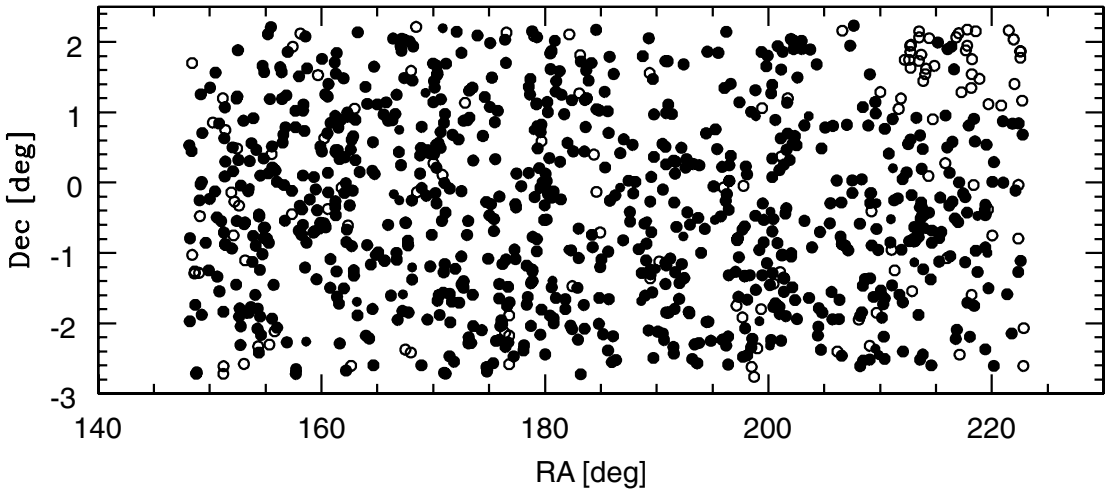

Figure 1. Projected distribution of radio sources with optical counterparts in the APM catalogue for $b_J \leqslant 19.45$. Filled circles identify objects with spectral identifications, while empty circles are for those not included in the 2dFGRS.

from the plots that these two classes of objects tend to occupy different regions of the b_J–S plane, star-forming sources being in general brighter in magnitude and fainter in radio flux. In spite of this difference, we see that the overwhelming majority of the spectroscopic sample has $r > 30$, i.e. the sample is made of radio-loud sources, regardless of the nature of the radio emission.

Radio luminosities have then been derived according to the relation $\mathcal{P} \equiv \mathrm{P}_{1.4\,\mathrm{GHz}} = S_{1.4\,\mathrm{GHz}} D^2 (1+z)^{3+\alpha}$, and are expressed in (W Hz^{-1} sr^{-1}) units. In the above formula, D is the angular diameter distance and α is the spectral index of the radio emission ($S(\nu) \propto \nu^{-\alpha}$). Following Magliocchetti et al. (2002), we assumed $\alpha = 0.5$ for Seyfert 1 galaxies, $\alpha = 0.75$ for early-type galaxies (with or without emission lines due to AGN activity), $\alpha = 0.7$ for Seyfert 2 galaxies and $\alpha = 0.35$ both for late-type galaxies and starbursts. Fig. 3 shows the resulting distribution of radio luminosities for the whole spectroscopic sample (lower panel) and for the subclass of radio-AGNs (top panel). The lack of objects at $\log_{10}\mathcal{P} \lesssim 21$–$21.5$ seen in the distribution of AGN-fuelled sources is not seen in the whole spectroscopic sample because of the population of low-luminosity star-forming galaxies which are limited to radio powers $\log_{10}\mathcal{P} \lesssim 22$ (see also Magliocchetti et al. 2002). We also note that all the sources in our sample have moderate luminosities ($\mathcal{P} \lesssim 10^{24}$), i.e. that all the AGN-fuelled objects belong to the class of Fanaroff–Riley type I (FR I) galaxies (Fanaroff & Riley 1974). This is as expected, because the local radio luminosity function of steep spectrum sources drops rapidly at $\mathcal{P} \gtrsim 10^{25}$ (Dunlop & Peacock 1990), which is the typical minimum luminosity of an FR II galaxy.

With the aim of studying the clustering properties of the population of local radio sources, following Hawkins et al. (2003) and Madgwick et al. (2003) we have discarded from the original FIRST–2dFGRS sample all the radio objects in 2dFGRS fields with <70 per cent completeness. Furthermore, we have also only considered those sources with redshifts $0.01 < z < 0.3$ and magnitudes $b_J \leqslant 19.37$. This magnitude limit is the brightest over the area of the 2dFGRS survey (Colless et al. 2001, 2003), and so using this limit over the whole area removes the need to correct for variations in the magnitude limit. These cuts leave us with a total of 761 objects (spectroscopic sample) out of which 536 belong to the population of AGN-fuelled sources (radio-AGN sample). Their redshift distributions are illustrated by the histograms in Fig. 4.

3.2 Redshift-space correlation function

The standard way to quantify the clustering properties of a particular class of sources is by means of the two-point correlation function ξ, which measures the excess probability of finding a pair in the two volume elements $\mathrm{d}V_1$ and $\mathrm{d}V_2$ separated by a distance r. In practice, ξ is obtained by comparing the actual source distribution

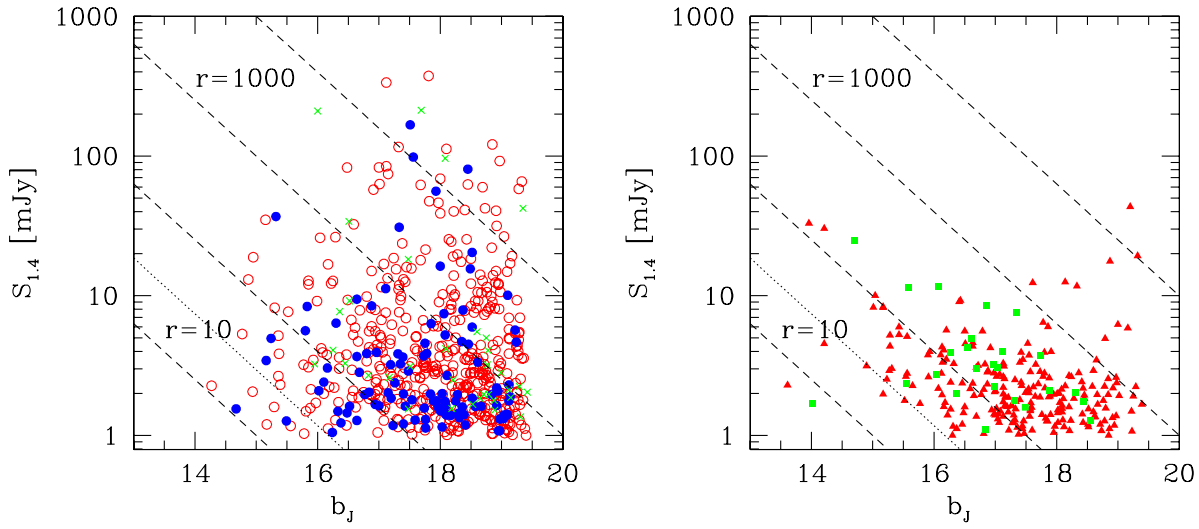

Figure 2. b_J magnitudes versus radio flux S at 1.4 GHz for different classes of objects. The left-hand panel shows the case for early-type galaxies (represented by empty circles), E+AGN-type galaxies (filled circles) and Seyfert galaxies (crosses), while the right-hand panel is obtained for the populations of late-type galaxies (filled triangles) and starbursts (filled squares). Dashed lines correspond to constant values of the radio-to-optical ratio $r = 10, 100, 10^3, 10^4$; the dotted lines indicate the threshold of $r \sim 30$ for radio-loudness.

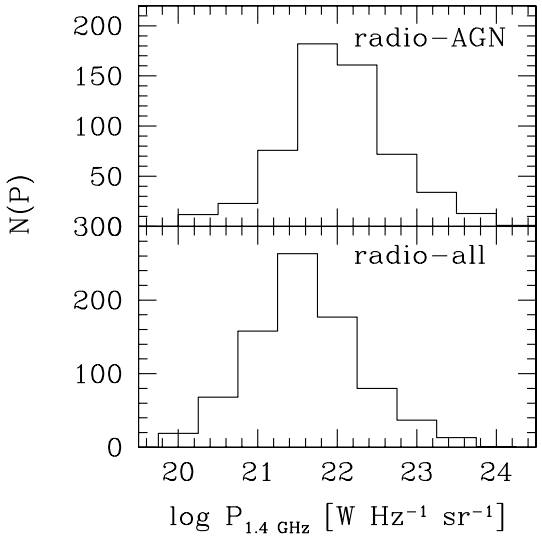

Figure 3. Distribution of monochromatic radio power at 1.4 GHz for those FIRST radio sources identified in the 2dFGRS survey. The top panel only includes objects that present signatures of AGN activity in their optical spectra, while the bottom panel is for the whole FIRST–2dFGRS sample.

with a catalogue of randomly distributed objects, subject to the same redshift and mask constraints as the real data. We chose to use the estimator (Hamilton 1993)

$$\xi(s) = 4\frac{DDRR}{(DR)^2} - 1, \qquad (1)$$

where DD, RR and DR are the number of data–data, random–random and data–random pairs separated by a distance s (note that throughout this section we will write the distance as s instead of r to stress the fact that we are working in redshift space).

We generated random catalogues with 10 times as many objects as the real data sets, and modulated the angular distribution by both the 2dFGRS and FIRST coverage maps, so that the instrumental window functions did not affect the measured clustering. The redshift distribution for these objects was then generated using the selection function of the different data sets under consideration. Equivalent $w_i(z) = 1/[1 + 4\pi n_R(z) J_3(s)] = 1$ (where $n_R(z)$ is the number density of radio sources at redshift z and $J_3 \equiv \int_0^s \xi(s') s'^2\, ds'$; see Hawkins et al. 2003; Madgwick et al. 2003) weights were assigned to each object both in the real and random catalogues. This assumption was justified by the extremely low number density of radio sources ($n_R(z)^{max} \simeq 6 \times 10^{-6}$ Mpc^{-3}) which makes the $4\pi n_R(z) J_3(s)$ contribution to w_i a negligible one for any sensible value of J_3.

The above procedure was repeated both for the whole spectroscopic sample and in the case of only radio-AGNs. The redshift distributions for the two random catalogues corresponding to the different samples are shown by the dashed lines in Fig. 4. The resulting redshift-space correlation functions $\xi(s)$ are shown in Fig. 5, where the left-hand panel is for the full spectroscopic sample, and the right-hand panel for radio-AGNs. The error bars on $\xi(s)$ were obtained by jack-knife resampling each data set 20 times.

Fig. 5 suggests that a universal power law is not a good fit on all scales for either of the measured $\xi(s)$ and that it is particularly poor for the AGN-powered sources. Although a power law fits well over the range $6 \lesssim s/[\mathrm{Mpc}] \lesssim 50$, the redshift-space correlation function steepens at larger scales, and flattens on smaller scales, particularly for the radio-AGN sample. We estimate the true value of the redshift-space correlation length s_0 by fitting a localized power law of the form $\xi(s) = (s/s_0)^{-\gamma_s}$ only in the range $6 \lesssim s/[\mathrm{Mpc}] \lesssim 50$.

The corresponding best values for the parameters s_0 and γ_s can be obtained by a χ^2 fit to ξ as a function of s. This analysis gives $s_0 = 10.7^{+0.8}_{-0.7}$ Mpc and $\gamma_s = 1.5 \pm 0.1$ for the whole FIRST–2dFGRS sample, while in the case of AGN sources we obtain $s_0 = 13 \pm 0.9$ Mpc and $\gamma_s = 1.8^{+0.1}_{-0.2}$. These best fits are shown by the dashed lines in Fig. 5. The dotted line on the left-hand panel of Fig. 5 shows the redshift-space correlation function for the entire population of 2dFGRS galaxies, derived by Hawkins et al. (2003); the similarity between this measurement and the one for local radio sources is remarkable. This can be understood because the FIRST–2dFGRS catalogue probes radio fluxes down to $S_{1.4\,GHz} = 1$ mJy, which results in a mixture of 'classical' AGN-fuelled sources, generally hosted by elliptical galaxies, and star-forming objects such as spirals and

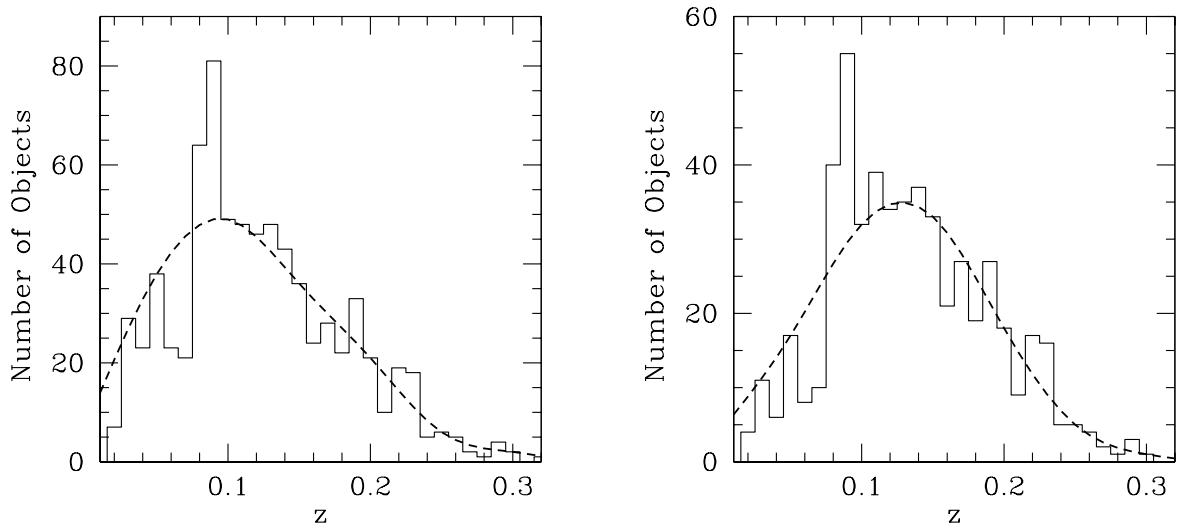

Figure 4. Left-hand panel: redshift distribution $N(z)$ for the whole spectroscopic sample (solid line) and for the normalized random catalogues (dashed line). Right-hand panel: same as before but for the class of radio-AGN sources (see text for details).

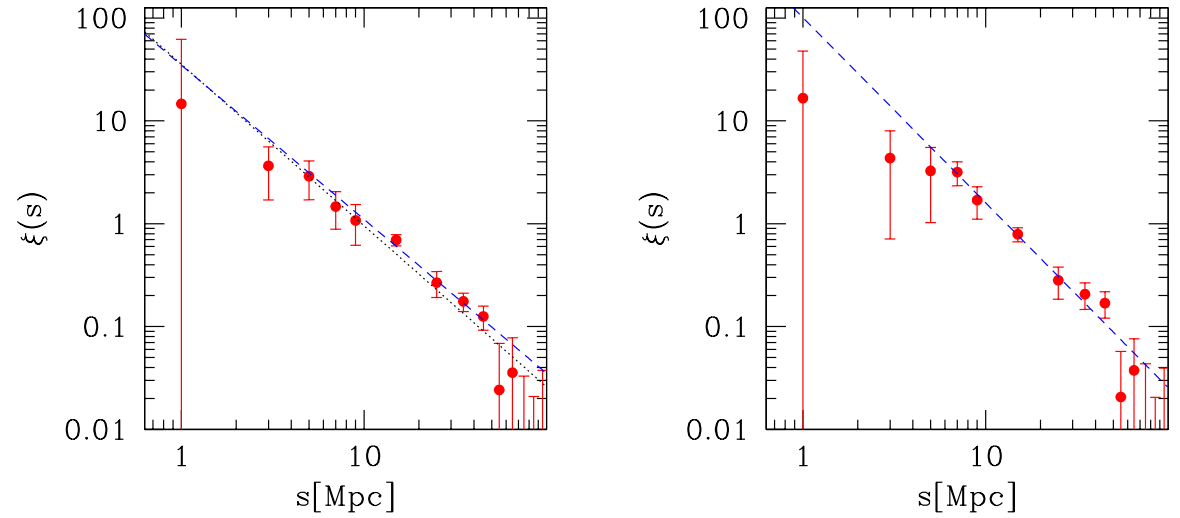

Figure 5. Left-hand panel: redshift-space correlation function for the whole spectroscopic sample (761 sources). Error bars are obtained via jack-knife resampling of the data set under consideration; given the large uncertainties associated with the smallest-scale measurement in the corresponding bin we only plot its upper limit. The dashed line represents the best fit to the data (derived only for those points included in the range $6 \lesssim s/[\mathrm{Mpc}] \lesssim 50$) corresponding to $\gamma_s = 1.5$ and $s_0 = 10.7$ Mpc, while the dotted line illustrates the best-fitting results found by Hawkins et al. (2003) for the entire population of 2dFGRS galaxies. Right-hand panel: redshift-space correlation function for the subsample of radio-AGNs (536 sources). Error bars are obtained as for the spectroscopic sample. The dashed line represents the best fit to the $6 \lesssim s/[\mathrm{Mpc}] \lesssim 50$ data, corresponding to $\gamma_s = 1.8$ and $s_0 = 13$ Mpc.

irregulars (see Section 2). This mix of early- and late-type galaxies makes the data set look similar to a fair (even though very sparse) sample of the whole population of 2dFGRS galaxies.

The situation however looks very different if we consider only AGN-fuelled sources. In this case the sample is much more strongly correlated; the correlation length is higher, and also $\xi(s)$ has a steeper slope. We will discuss the implications of these findings in Section 3.3 when dealing with the real-space correlation function.

As a final step, we are interested in investigating whether there is any dependence of the clustering signal on radio luminosity. We divided the radio-AGN sample into two distinct subsets depending on whether the sources have radio luminosity brighter or fainter than $\log_{10}\mathcal{P} = 22.0$. There are 260 objects in the faint sample, and their average radio luminosity is $\log_{10}\mathcal{P} = 22.9$. There are 276 objects in the bright sample, with average radio luminosity $\log_{10}\mathcal{P} = 21.6$.

The redshift-space correlation functions for the two samples are plotted in Fig. 6; the fainter sample is plotted as filled circles, and the brighter sample as open squares. Even though the small number of sources in the subsets leads to large uncertainties in the measurements, it is clear that the two $\xi(s)$ are entirely compatible with each other. The best-fitting parameters are $s_0 = 12 \pm 3$ Mpc and $\gamma_s = 1.5 \pm 0.15$ for brighter AGNs and $s_0 = 13 \pm 3$ Mpc and $\gamma_s = 1.4 \pm 0.1$ for the fainter ones. This result shows no evidence for luminosity dependence in the clustering amplitude, and shows that the amplitude of the correlation function at 10 Mpc cannot differ by more much than a factor of 2 even though the two samples differ by a factor of 20 in luminosity. This is consistent with the results of Peacock & Nicholson (1991) who analysed an all-sky sample of radio galaxies at $z \lesssim 0.1$, and found no evidence for any difference in clustering amplitude for samples $22.5 < \log_{10}\mathcal{P} < 23.5$ and

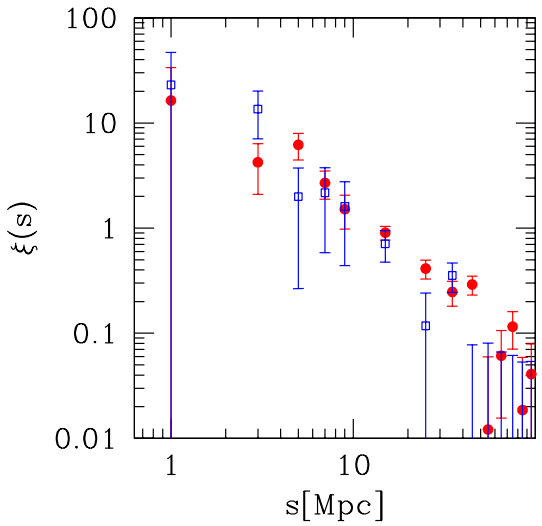

Figure 6. Redshift-space correlation function for the two subsamples of radio-AGNs respectively brighter (open squares) and fainter (filled circles) than $\log_{10}\mathcal{P} = 22$. Error bars are from Poisson noise estimates for the data set under consideration.

$23.5 < \log_{10}\mathcal{P} < 24.5$. These results imply that the correlation amplitude of radio galaxies is independent of their radio luminosity, at least in the power range $10^{20} \lesssim \mathcal{P} \lesssim 10^{25}$.

3.3 Projected correlation function

The previous section has shown that the redshift-space correlation function is extremely useful for characterizing the main properties of the clustering of low-redshift radio sources. However, $\xi(s)$ differs from the real-space correlation function because of peculiar velocities that lead to redshift-space distortions (see, for example, Hawkins et al. 2003; Madgwick et al. 2003). It follows that both the amplitude and the slope of the real-space correlation function $\xi(r)$ will differ from the values measured in Section 3.2.

The standard way to recover $\xi(r)$ is to first compute the two-dimensional correlations as a function of separation parallel and transverse to the line of sight, $\xi(r_\mathrm{P}, r_\mathrm{T})$ and then integrate it along the r_P direction in order to obtain the projected correlation function Ξ as

$$\Xi(r_\mathrm{T}) = 2\int_0^\infty \xi(r_\mathrm{P}, r_\mathrm{T})\,\mathrm{d}r_\mathrm{P}. \tag{2}$$

We estimate $\xi(r_\mathrm{P}, r_\mathrm{T})$ by means of equation (1) – where this time pairs are counted in a grid of bins Δr_P, Δr_T – and we derive Ξ by means of equation (2). We set the upper limit for the integral to $r_\mathrm{P}^\mathrm{max} = 60$ Mpc as the best compromise between a large enough value to produce stable results and a small enough value to avoid extra noise added to Ξ.

As in the previous subsection, Ξ has been evaluated using both the whole spectroscopic sample and the sample of objects showing signatures of AGN in their spectra. Once again, the errors were calculated from 20 jack-knife resamplings of the data sets under consideration.

The resulting measurements on scales of 1–30 Mpc are shown by the solid points in the two panels of Fig. 7: the left-hand panel shows the results for the whole spectroscopic sample, and the right-hand panel shows the results for the AGN sample. The open squares in Fig. 7 show the projected correlation functions from corresponding optical 2dFGRS samples: in the left-hand panel they show the results for the entire population of 2dF galaxies (Hawkins et al. 2003); in the right-hand panel they show the results for early-type 2dFGRS galaxies (Madgwick et al. 2003). From these comparisons we see that the clustering properties of the whole spectroscopic sample are remarkably similar to those of 'normal' galaxies, but the projected correlation function of radio-AGNs has an amplitude that is roughly twice as large as that of local ellipticals.

From the measurements presented in Fig. 7 it is then possible to estimate the real-space correlation function $\xi(r)$ via (Davis & Peebles 1983)

$$\Xi(r_\mathrm{T}) = 2\int_{r_\mathrm{T}}^\infty \xi(r)\frac{r\,\mathrm{d}r}{\left(r^2 - r_\mathrm{T}^2\right)^{1/2}} \tag{3}$$

which, if we assume the power-law form $\xi(r) = (r/r_0)^{-\gamma}$, can be integrated analytically leading to

$$\Xi(r_\mathrm{T}) = r_0^\gamma\, r_\mathrm{T}^{1-\gamma}\, H_\gamma, \tag{4}$$

where $H_\gamma = \Gamma(1/2)\Gamma[(\gamma-1)/2]/\Gamma(\gamma/2)$.

A least-squares fit to the data for the whole spectroscopic sample gives $r_0 = 6.7^{+0.9}_{-1.1}$ Mpc, $\gamma = 1.6 \pm 0.1$, surprisingly close to the results of Hawkins et al. (2003). For the AGN population we find $r_0 = 10.9^{+1.0}_{-1.2}$ Mpc, $\gamma = 2.0 \pm 0.1$, which is similar to that found by Norberg et al. (2002) for the brightest early-type galaxies in the 2dFGRS. A summary of the results derived here and in Section 3.2 can be found in Table 2.

We note that a measured correlation length $r_0 \simeq 11$ Mpc is in very good agreement with previous estimates derived from deprojection of the angular two-point correlation function $w(\theta)$. These include the results of Cress et al. (1996), Loan et al. (1997), Magliocchetti et al. (1998) and Magliocchetti & Maddox (2002). However, more recent works (e.g. Blake & Wall 2002; Overzier et al. 2003) seem to find lower values for r_0, of the order of 5–6 h^{-1} Mpc. Given that the functional form for the redshift distribution of radio sources at the mJy level adopted by the various authors is the same, i.e. the one proposed by Dunlop & Peacock (1990), we ascribe the differences found by Blake & Wall (2002) and Overzier et al. (2003) as caused by not properly dealing with the issue of multicomponent sources. Ignoring the effect of multiple sources on the observed clustering properties of radio objects in fact leads (amongst others) to an underestimate of the slope of $w(\theta)$, $1-\gamma$, which in turn yields smaller inferred values for the correlation length r_0.

4 CONSTRAINTS ON THE HALO AND BLACK HOLE MASS

Because the Ξ measurements presented in the right-hand panel of Fig. 7 have been obtained for a homogeneous sample of AGN-fuelled sources, we can easily predict the clustering for a range of models to be directly compared with the data.

Table 2. Best-fitting parameters to ξ. In the case of $\xi(s) = (s/s_0)^{-\gamma_s}$ the fit only uses points with $6 \lesssim s/[\mathrm{Mpc}] \lesssim 50$ Mpc, while for r_0 and γ all the points between $r_\mathrm{T} = 1$ and $r_\mathrm{T} = 30$ Mpc have been considered.

	Whole sample	Radio-AGN
s_0 (Mpc)	$10.7^{+0.8}_{-0.7}$	13 ± 0.9
γ_s	1.5 ± 0.1	$1.8^{+0.1}_{-0.2}$
r_0 (Mpc)	$6.7^{+0.9}_{-1.1}$	$10.9^{+1.0}_{-1.2}$
γ	1.6 ± 0.1	2.0 ± 0.1

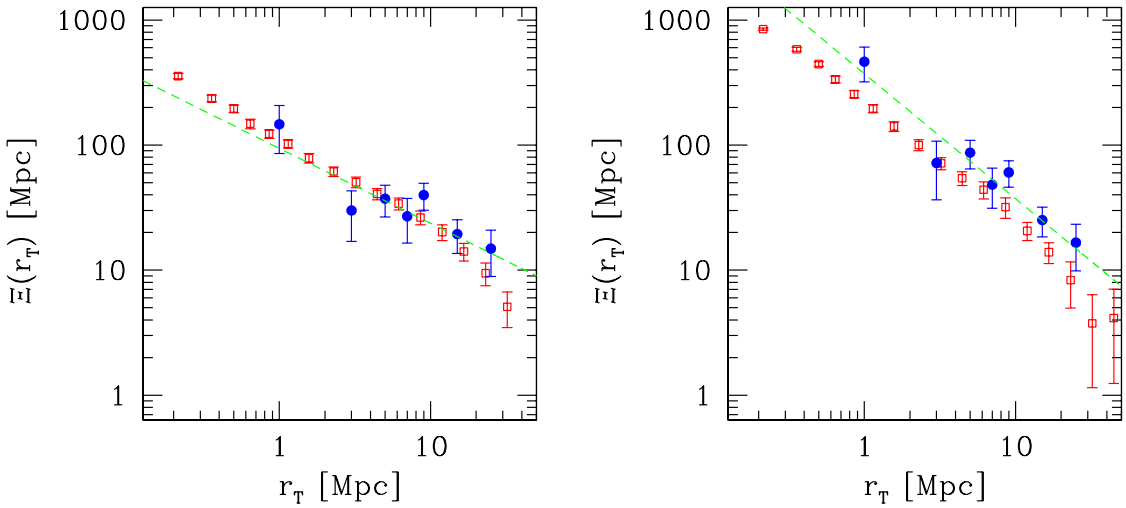

Figure 7. Left-hand panel: projected correlation function for the whole spectroscopic sample (761 sources). Error bars are obtained as jack-knife resampling of the data set under consideration. The dashed line represents the best fit to the data corresponding to $\gamma = 1.6$ and $r_0 = 6.7$ Mpc, while open squares illustrate the results obtained by Hawkins et al. (2003) for the entire population of 2dFGRS galaxies. Right-hand panel: projected correlation function for the subsample of radio-AGNs (536 sources). Error bars are obtained as for the spectroscopic sample. The dashed line represents the best fit to the data corresponding to $\gamma = 2.0$ and $r_0 = 10.9$ Mpc, while open squares illustrate the results obtained by Madgwick et al. (2003) for the population of early-type 2dFGRS galaxies.

Under the assumption that each dark matter halo can only host one radio-AGN (but see later for a more general discussion), the predicted spatial correlation function ξ (on a scale r and at a redshift z) for this class of sources can in fact be written as

$$\xi(r, z) = \xi_{\rm dm}(r, z) b^2_{\rm eff}(\mathrm{M_{min}}, z). \quad (5)$$

This expression holds on scales $\gtrsim$1 Mpc where the halo–halo exclusion effects are negligible (for the general case see Magliocchetti & Porciani 2003).

The mass–mass correlation function $\xi_{\rm dm}(r, z)$ in equation (5) is fully specified for a given cosmological model and a chosen normalization σ_8. The precise form of $\xi_{\rm dm}(r, z)$ can be analytically derived following the approach of Peacock & Dodds (1996). The effective bias $b_{\rm eff}(\mathrm{M_{min}}, z)$, which determines the way radio sources trace the mass distribution, is obtained via

$$b_{\rm eff}(\mathrm{M_{min}}, z) = \frac{\left[\int_{\mathrm{M_{min}}}^{\infty} b(m, z) n(m, z)\, \mathrm{d}m\right]}{\left[\int_{\mathrm{M_{min}}}^{\infty} n(m, z)\, \mathrm{d}m\right]}, \quad (6)$$

where $b(m, z)$ and $n(m, z)$ respectively are the linear bias factor and the halo mass function of individual haloes of mass m at a redshift z and – in our specific case – $\mathrm{M_{min}}$ is the minimum mass of a halo able to host a radio-AGN.

In order to compare models with data we have then written both $b(m, z)$ and $n(m, z)$ according to the Sheth & Tormen (1999) prescriptions and derived the theoretical projected Ξ by integrating the spatial correlation function (5) along the direction parallel to the line of sight $r_{\rm P}$ via equation (3), where all the relevant quantities are evaluated at the median redshift of the 2dFGRS, $\langle z \rangle \simeq 0.1$.

The dotted lines in Fig. 8 show the predictions obtained from equation (5) for different values of the minimum halo mass necessary to host a radio-AGN as compared to the measurements derived in Section 3.3. The chosen values for the minimum mass range from $\mathrm{M_{min}} = 10^{10}\ \mathrm{M_\odot}$ (bottom dotted curve) to $10^{14}\ \mathrm{M_\odot}$ (top dotted curve). Despite the large error bars, it is clear that none of the predicted Ξ for minimum halo masses $\lesssim 10^{13}\ \mathrm{M_\odot}$ can provide a reasonable fit to the data, because they all fall below the observed values. Indeed, the best fit is obtained for $\log_{10}[\mathrm{M_{min}}/\mathrm{M_\odot}] = 13.7^{+0.2}_{-0.3}$,

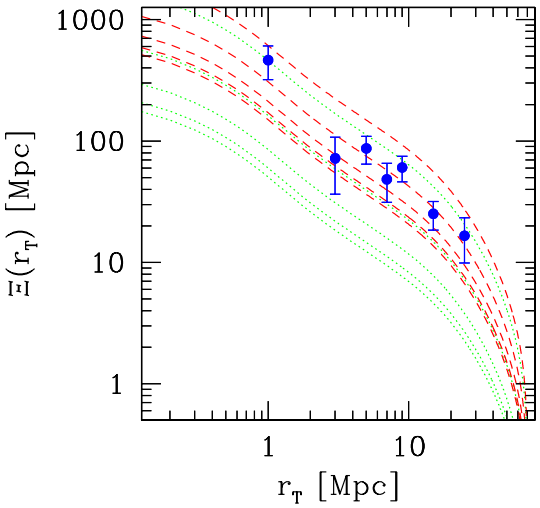

Figure 8. Projected correlation function of radio-AGNs. Measurements are those obtained in Section 3.3, while the dotted lines show the predictions derived from equation (5) for minimum halo masses ranging from 10^{10} (bottom curve) to 10^{14} (top curve) $\mathrm{M_\odot}$. Dashed lines are obtained as in the former case but for a mean halo occupation number $\langle N_{\rm radio} \rangle \propto m$ (see text for details).

corresponding to an effective bias $b_{\rm eff} = 1.85$. We note that very similar values (i.e. $\log_{10}[\mathrm{M_{min}}/\mathrm{M_\odot}] = 13.5^{+0.2}_{-0.3}$ and $\log_{10}[\mathrm{M_{min}}/\mathrm{M_\odot}] = 13.0^{+0.3}_{-0.5}$) are also found if we release the assumption of one radio galaxy per halo and consider more general distributions of the kind $\langle \mathrm{N_{radio}} \rangle \propto m^{0.5}$ (see, for example, Peacock 2003) or a more extreme $\langle \mathrm{N_{radio}} \rangle \propto m$ (where $\langle \mathrm{N_{radio}} \rangle$ is the average number of radio galaxies per halo of mass m) even though, as expected, the difference between models derived for different values of $\mathrm{M_{min}}$ decreases as we increase the weight given to larger-mass haloes (see Fig. 8).

The implications of the above results are quite intriguing because they suggest, independent of the chosen halo occupation form, that radio-AGNs reside in relatively massive haloes, spanning a mass range from rich groups to supermassive clusters. Smaller haloes

seem to be inhibited from hosting a radio-emitting AGN. This conclusion is also supported by the small-scale behaviour of the redshift-space correlation function of radio-AGNs as measured in Section 3.2. Indeed, both the lack of pairs with distance $\lesssim$1 Mpc and the flattening of $\xi(s)$ on scales $\lesssim$5 Mpc have a natural explanation if we assume AGN-powered sources to be confined in massive haloes (even if we cannot exclude this latter finding as due to the Finger of God effect; see Hawkins et al. 2003). In the case where only one source per halo is assumed, the halo–halo spatial exclusion ensures that no pair of radio-AGNs can be found with a separation smaller than the sum of the virial radii of the haloes that host them. For a typical halo mass of $10^{13.4}$ $M_\odot$ the minimum separation for the adopted cosmology turns out to be $\sim$1.6 Mpc. Allowing for the uncertainties in our determination of M_{min}, this implies that there should be a deficit of pairs on scales $\sim$1–5 Mpc, consistent with the observed flattening of $\xi(s)$ on small scales.

Thus, our average estimate of the minimum halo mass for a radio-AGN is $\log_{10}[M_{min}/M_\odot] \simeq 13.4$), which is about a factor of 10 larger than that associated with 'normal' early-type galaxies, $\log_{10}[M_{min}/M_\odot] \simeq 12.5$ (Magliocchetti & Porciani 2003). This is also about a factor of 10 larger than that obtained for the population of radio-quiet quasars in the 2dF quasi-stellar object (QSO) data set, $\log_{10}[M_{min}/M_\odot] \simeq 12.1$–$12.6$ (Grazian et al. 2004). All three of the above determinations are based on samples drawn from the same parent catalogue (APM survey), and so selection effects are not expected to bias the comparison between the different results.

Taking these numbers at face value suggests that radio-AGNs and radio-quiet quasars are two distinct populations, with more massive dark matter haloes required for an AGN to trigger radio activity.

On the other hand, the results presented in Section 3.2 (see Fig. 6) together with those obtained by Peacock & Nicholson (1991) for more luminous radio galaxies show that radio-AGNs with very different radio luminosities have very similar correlation amplitude. If one thinks in terms of the model expressed in equation (5), there appears to be little or no correlation between radio luminosity and minimum halo mass. A simple comparison of Figs 6 and 8 illustrates that the correlation function estimates obtained for low-luminosity and moderately bright-luminosity radio-AGNs both fall in the same $10^{13} \lesssim M_{min}/M_\odot \lesssim 10^{14}$ range as found for the whole sample.

If we then combine the above information, the data seem to suggest that there is a threshold halo mass required to produce significant radio emission from an AGN but – once the radio activity is triggered – there seems to be no connection between radio luminosity of the sources and dark matter content of those haloes hosting them. Note that this statement does not necessarily imply the minimum halo mass to be the only factor playing a relevant role in the onset of radio emission from an AGN. Also, the threshold may not be a sharp mass threshold, but could be as a smooth transition between the radio-quiet and radio-loud regimes for haloes near M_{min}.

These results on the minimum halo mass can also be viewed in terms of a minimum black hole mass. Ferrarese (2002) gives a simple prescription to convert the dark matter mass M_{DM} of a halo hosting a black hole into black hole mass M_{BH}:

$$\frac{M_{BH}}{10^8\,M_\odot} \simeq 0.10 \left(\frac{M_{DM}}{10^{12}\,M_\odot}\right)^{1.65}. \quad (7)$$

Thus, a minimum halo mass $M_{min} \sim 10^{13.4}$ $M_\odot$ corresponds to $M_{min}^{BH} \sim 10^9$ $M_\odot$, which would represent the minimum black hole mass required to onset radio-AGN activity – at least for relatively faint/FR I sources such as the overwhelming majority of those we have considered in our analysis (see Section 3.1). It is interesting to note that this estimate is in good agreement with both the results of Marchesini, Celotti & Ferrarese (2004) and also those of Dunlop et al. (2003), despite the entirely different methods used in our analysis. Also our minimum black hole mass is noticeably larger than that obtained for radio-quiet quasars; from an analysis of the 2dF QSO data set in the same redshift range spanned by the sources considered in this work, Corbett et al. (2003) find $6.5 \lesssim \log_{10}[M_{BH}/M_\odot] \lesssim 8.3$. By making use of equation (7), we can then conclude that – at least for moderately faint/FR I radio sources – there seems to be a minimum black hole mass of about 10^9 $M_\odot$ required to produce significant radio emission from an AGN; however, once the radio emission is produced, there is little or no correlation between radio luminosity and black hole mass. This is in agreement with other analyses of radio-loud quasars by Dunlop et al. (2003) and Cirasuolo et al. (2003).

We note that, even though the connection between black hole mass and radio power has been obtained in our analysis as a consequence of the connection between radio power and halo mass, this first relationship is supposed to be more fundamental and physically based as it is the black hole which actually powers the AGN. Any correlation between radio power and halo mass is then expected to arise as a secondary effect, because black hole mass is observed to scale with bulge luminosity and this is turn is related – in the case of elliptical galaxies – to halo mass (see, for example, Magorrian et al. 1998; Kormendy & Gebhardt 2001; Archibald et al. 2002; McLure & Dunlop 2002; Granato et al. 2004).

5 CONCLUSIONS

This paper has presented the clustering properties of local, $S_{1.4\,GHz} \geqslant 1$ mJy radio sources by making use of a sample of 820 objects drawn from the joint use of the FIRST survey and the 2dFGRS. To this aim, we have introduced 271 new $b_J \leqslant 19.45$ spectroscopic counterparts for FIRST radio sources to be added to those already obtained by Magliocchetti et al. (2002). These objects can be divided into two broad subclasses: (1) star-forming objects (66 sources, which include both late-type and star-burst galaxies), which owe their radio activity to processes connected to intense star formation; (2) radio-AGNs (202 sources), where the radio signal stems from accretion processes on to a central black hole. In both cases, the redshift range spanned extends up to $z \simeq 0.3$ (with star-forming objects being relatively more local than AGN-fuelled sources) and radio luminosities cover the interval $10^{20} \lesssim \mathcal{P} \lesssim 10^{24}$, which identifies the radio-AGNs included in the sample as FR I sources.

The redshift-space correlation function $\xi(s)$ and the projected correlation function $\Xi(r_T)$ have been calculated for both the total FIRST–2dFGRS sample and for the subclass of radio-AGNs. The results for the two populations are quite different.

In the case of all FIRST–2dFGRS sources, both the correlation functions are found to be entirely consistent with the estimates obtained by Hawkins et al. (2003) for the whole sample of 2dFGRS galaxies. From measurements of the redshift-space correlation function $\xi(s)=(s/s_0)^{-\gamma_s}$ we derive a redshift-space clustering length $s_0 = 10.7^{+0.8}_{-0.7}$ Mpc and a slope $\gamma_s = 1.5 \pm 0.1$, while from the projected correlation function $\Xi(r_T)$ we estimate the parameters of the real-space correlation function $\xi(r) = (r/r_0)^{-\gamma}$ to be $r_0 = 6.7^{+0.9}_{-1.1}$ Mpc and $\gamma = 1.6 \pm 0.1$.

Sources that show signatures of AGN activity in their spectra are found to be very strongly clustered, with a value for the redshift-space clustering length, $s_0 = 13.0 \pm 0.9$ (Peacock & Nicholson 1991). Measurements of the real-space correlation function lead to $r_0 \simeq 11$ Mpc and $\gamma \simeq 2$, slightly steeper and higher amplitude

than optically selected galaxies, but very similar to bright early-type galaxies.

We also find no significant differences in the clustering properties of faint ($\mathcal{P} \leqslant 10^{22}$) compared to brighter ($\mathcal{P} > 10^{22}$) AGN-fuelled radio sources.

Comparisons with physically-motivated models for the clustering properties of classes of galaxies show that AGN-fuelled sources have to reside in dark matter haloes more massive than $\log_{10}[M_{\rm min}/{\rm M}_{\odot}] \simeq 13.4$, higher than the figure recently measured for radio-quiet QSOs (see, for example, Grazian et al. 2004). Under certain assumptions, this value can be converted into a minimum black hole mass associated with radio-loud, AGN-fuelled objects of $M_{\rm BH}^{\rm min} \sim 10^9$ M$_{\odot}$, again larger than current estimates for the typical black hole mass associated with local 2dF (radio-quiet) quasars (Corbett et al. 2003).

The above results then suggest – at least for moderately faint/FR I radio sources such as those included in our sample – the existence of a threshold halo/black hole mass associated with the onset of significant radio activity such as that of radio-loud AGNs. We stress that such a threshold is not necessarily a sharp one, as it could as well identify an allowed range (in the high-mass regime) for the transition between radio-quiet and radio-loud regimes. Once the activity is triggered there seems to be no evidence for a connection between halo/black hole mass and radio luminosity.

REFERENCES

Archibald E. N., Dunlop J. S., Jimenez R., Friaca A. C. S., McLure R. J., Hughes D. H., 2002, MNRAS, 336, 353

Auriemma C., Perola G. C., Ekers R., Fanti R., Lari C., Jaffe W. J., Ulrich M. H., 1977, A&A, 57, 41

Becker R. H., White R. L., Helfand D. J., 1995, ApJ, 450, 559

Blake C., Wall J. V., 2002, MNRAS, 329, L37

Blake C., Wall J. V., 2003, MNRAS, 337, 993

Cirasuolo M., Magliocchetti M., Celotti A., Danese L., 2003, MNRAS, 341, 993

Colless M. et al., (2dFGRS Team), 2001, MNRAS, 328, 1039

Colless M. et al. (2dFGRS Team), 2003, preprint (astro-ph/0306581)

Condon J. J., Cotton W. D., Greisen E. W., Yin Q. F., Perley R. A., Taylor G. B., Broderick J. J., 1998, AJ, 115, 1693

Corbett E. A. et al. 2003, MNRAS, 343, 705

Cress C. M., Helfand D. J., Becker R. H., Gregg M. D., White R. L., 1996, ApJ, 473, 7

Davis M., Peebles P. J. E., 1983, ApJ, 208, 13

Dunlop J. S., Peacock J. A., 1990, MNRAS, 247, 19

Dunlop J. S., McLure R. J., Kukula M. J., Baum S. A., O'Dea C. P., Hugher D. H., 2003, MNRAS, 340, 1095

Falomo R., Carangelo N., Treves A., 2003, MNRAS, 343, 505

Fanaroff B. L., Riley J. M., 1974, MNRAS, 167, L31

Ferrarese L., 2002, ApJ, 578, 90

Granato G. L., De Zotti G., Silva L., Bressan A., Danese L., 2004, ApJ, 600, 580

Grazian A., Negrello M., Moscardini L., Cristiani S., Haenelt M. G., Matarrese S., Omizzolo A., Vanzella E., 2004, AJ, 127, 592

Hamilton A. J. S., 1993, ApJ, 417, 19

Hawkins E. et al., (2dFGRS Team), 2003, MNRAS, 346, 78

Hill T. L., Heisler C. A., Norris R. P., Reynolds J. E., Hunstead R. W., 2001, ApJ, 548, 127

Kennicut R. C., 1992, ApJ, 388, 310

Kooiman L. K., Burns J. O., Klypin A. A., 1995, ApJ, 448, 500

Kormendy J., Gebhardt K., 2001, in Weeler J. C., Martel H., eds, Proc. AIP Conf. Vol. 586, 20th Texas Symposium on Relativistic Astrophysics. American Institute of Physics, New York, p. 363

Lacy M., Laurent-Muehleisen S. A., Ridgway S. E., Becker R. H., White R. L., 2001, ApJ, 551, L17

Lahav O. et al., (2dFGRS Team), 2002, MNRAS, 333, 961

Laor A., 2000, ApJ, 543, L111

Loan A. J., Wall J. V., Lahav O., 1997, MNRAS, 286, 994

McLure R. J., Dunlop J. S., 2002, MNRAS, 331, 795

McLure R. J., Jarvis M. J., 2002, MNRAS, 337, 109

McQuade K., Calzetti D., Kinney A. L., 1995, ApJS, 97, 331

Maddox S. J., Efstathiou G., Sutherland W. J., Loveday J., 1990a, MNRAS, 243, 692

Maddox S. J., Efstathiou G., Sutherland W. J., 1990b, MNRAS, 246, 433

Maddox S. J., Efstathiou G., Sutherland W. J., 1996, MNRAS, 283, 1227

Madgwick D. S. et al., (2dFGRS Team), 2003, MNRAS, 344, 847

Magliocchetti M., Maddox S. J., 2002, MNRAS, 330, 241

Magliocchetti M., Porciani C., 2003, MNRAS, 346, 186

Magliocchetti M., Maddox S. J., Lahav O., Wall J. V., 1998, MNRAS, 300, 257

Magliocchetti M., Maddox S. J., Lahav O., Wall J. V., 1999, MNRAS, 306, 943

Magliocchetti M. et al., (2dFGRS Team), 2002, MNRAS, 333, 100

Magorrian J. et al., 1998, AJ, 115, 2285

Marchesini D., Celotti A., Ferrarese L., 2004, MNRAS, in press (astro-ph/0403272)

Norberg P. et al., (2dFGRS Team), 2002, MNRAS, 332, 827

Overzier R. A., Rottgering H. J. A., Rengelink R. B., Wilman R. J., 2003, A&A, 405, 53

Peacock J. A., 2003, preprint (astro-ph/0309240)

Peacock J. A., Dodds S. J., 1996, MNRAS, 267, 1020

Peacock J. A., Nicholson D., 1991, MNRAS, 253, 307

Rengelink R. B., Myley G. K., Rottgering H. J. A., Bremer M. N., de Bruyn A. G., Tang Y., 1998, in Bremer M., Jackson N., Perez-Fournon I., eds, Observational Cosmology with the New Radio Surveys. Kluwer, Dordrecht, p. 143

Rola C., Terlevich E., Terlevich R., 1997, MNRAS, 289, 419

Seldner M., Peebles P. J. E., 1981, MNRAS, 194, 251

Shaver P. A., Pierre M., 1989, A&A, 220, 35

Sheth R. K., Tormen G., 1999, MNRAS, 308, 119

Spergel D. N. et al., 2003, ApJS, 148, 175

Veilleux S., Osterbrock D. E., 1987, ApJ, 63, 295

Woltjer L., 1990, in Blandford R., Netzer H., Woltjer L., eds, Saas-Fee Advanced Course 20, Active Galactic Nuclei. Springer-Verlag, Berlin

This paper has been typeset from a TEX/LATEX file prepared by the author.